www.czasopisma.pan.pl PAN POLSKA AKADEMIA NAUK www.journals.pan.pl

PAN ARCHIVES OF ACOUSTICS
Vol. **42**, No. 1, pp. 37–48 (2017)

DOI: 10.1515/aoa-2017-0005

2D Structural Acoustic Analysis Using the FEM/FMBEM with Different Coupled Element Types

Leilei CHEN[(1)], Wenchang ZHAO[(2)], Cheng LIU[(2)], Haibo CHEN[(2)]

[(1)] *College of Civil Engineering, Xinyang Normal University*
Xinyang 464000, Henan, P.R.China; e-mail: chenllei@mail.ustc.edu.cn

[(2)] *Department of Modern Mechanics*
University of Science and Technology of China
CAS Key Laboratory of Mechanical Behavior and Design of Materials
Hefei 230026, Anhui, P.R.China; e-mail: {JsuKya, chengliu, hbchen}@ustce.edu.cn

(*received June 16, 2016; accepted October 19, 2016*)

A FEM-BEM coupling approach is used for acoustic fluid-structure interaction analysis. The FEM is used to model the structure and the BEM is used to model the exterior acoustic domain. The aim of this work is to improve the computational efficiency and accuracy of the conventional FEM-BEM coupling approach. The fast multipole method (FMM) is applied to accelerating the matrix-vector products in BEM. The Burton-Miller formulation is used to overcome the fictitious eigen-frequency problem when using a single Helmholtz boundary integral equation for exterior acoustic problems. The continuous higher order boundary elements and discontinuous higher order boundary elements for 2D problem are developed in this work to achieve higher accuracy in the coupling analysis. The performance for coupled element types is compared via a simple example with analytical solution, and the optimal element type is obtained. Numerical examples are presented to show the relative errors of different coupled element types.

Keywords: boundary element method; finite element method; discontinuous boundary elements; acoustic fluid-structure interaction; fast multipole method.

1. Introduction

The acoustic fluid-structure interaction is a classical problem in underwater acoustics. The sound pressure surrounding structures always has a big impact on the dynamic behavior of the structures, then the interaction between structures and fluid needs to be taken into account. Thus, developing effective numerical methods is necessary due to the impossibility of obtaining analytical solutions for realistic problems. The finite element method (FEM) is widely used for the simulation of the dynamic behavior of structures. However, the boundary element method (BEM) offers the advantage over the FEM for acoustic problems, because it provides an excellent accuracy and easy mesh generation. Moreover, the Sommerfeld radiation condition at infinity is automatically satisfied for exterior acoustic problems. Making the best use of the advantages of both methods, the FEM-BEM coupling approach was developed by Everstine, Henderson (1990), and the coupled approach has been widely adopted (Chen *et al.*, 1998; Rajakumar, Ali, 1996; Márquez *et al.*, 2004; Fritze *et al.*, 2005; Schneider, 2008).

It is well-known that the different element types always result in different performance, and the discontinuous elements outperform the continuous elements in many cases, because the discontinuous elements provide easy treatment of discontinuity, such as corners and edges. The comparison of different element types for BEM has been made in details. The performance of constant, linear, and quadratic boundary elements in the analysis of the 3D scattering problem was evaluated in (Tadeu, António, 2000), and the authors found that linear boundary elements outperform the constant and quadratic elements. Error dependence in terms of frequency, element size, and location of nodes on discontinuous elements is presented by Marburg, Schneider (2003), and the use of discontinuous quadratic elements is recommended. For discontin-

uous elements, interpolation nodes are located inside the element and element performance depends on the position of the interpolation nodes. The optimal values of the nodal position for discontinuous elements were recommended at the zeros of the Legendre polynomials in general (Marburg, Schneider, 2003). However, few papers compared the performance of the different element types for coupled FEM/BEM. Peters *et al.* (2012) used discontinuous linear boundary element with quadratic geometric interpolation coupled with eight-node isoparametric finite element to solve the 3D fluid structure interaction. Zhang, Zhang (2002) used discontinuous BEM coupled with FEM for elastostatics and fluid-structure interaction.

In this study, different coupled element types are used for fluid-structure interaction analysis, and their performance is investigated to obtain a proper scheme. Besides, an investigation on boundary element types and the optimal position of interpolation nodes in discontinuous element without FEM coupling is also done in this work. The Burton-Miller formulation (Burton, Miller, 1971) consisting of a linear combination of the conventional boundary integral equation and its normal derivative equation is applied to overcoming the nonuniqueness problem. And the Cauchy principal value and the Hadamard finite part integral method are applied to dealing with the strong singular and hyper-singular integrals. For different boundary element types, the non-singular expressions of boundary integral equations are presented in this work. On the other hand, the fast multipole method (FMM) is introduced to accelerate the calculation of BEM in (Coifman *et al.*, 1993; Chen *et al.*, 2013b; Wu *et al.*, 2011; Yu *et al.*, 2012; Li, Huang, 2011). However, constant boundary element used in (Coifman *et al.*, 1993; Chen *et al.*, 2013b; Wu *et al.*, 2011; Yu *et al.*, 2012; Li, Huang, 2011) will produce a solution with a low accuracy. In this paper, FMM is applied to discontinuous boundary element with quadratic shape function in order to improve the computational accuracy of the conventional boundary element. So, the proposed algorithm performs more efficiently than the conventional method in (Coifman *et al.*, 1993; Chen *et al.*, 2013b; Wu *et al.*, 2011; Yu *et al.*, 2012; Li, Huang, 2011).

2. Structural-acoustic analysis

2.1. BEM for acoustic domain

Consider the following Helmholtz equation governing the acoustic wave domain:

$$\nabla^2 p(x) + k^2 p(x) = 0, \quad \forall x \in \Omega, \tag{1}$$

where ∇^2 is the Laplace operator, p is the acoustic pressure, $k = \omega/c$ is the wave number, ω is the angular frequency, and c is the wave speed in the acoustic medium Ω. The boundary conditions can be classified as follows:

$$p(x) = \overline{p}(x), \qquad x \in S_p, \tag{2}$$

$$q(x) = \frac{\partial p(x)}{\partial n(x)} = i\rho\omega\overline{v}(x), \qquad x \in S_q, \tag{3}$$

$$p(x) = zv(x), \qquad x \in S_z, \tag{4}$$

where n denotes the outward unit normal vector to boundary S at point x; ρ is the medium density, $v(x)$ is the normal velocity, and z is the acoustic impedance. The quantities with overbars indicate given values on the boundary condition. S_p denotes the Dirichlet boundary condition, S_q denotes the Neumann boundary condition, and S_z denotes the Robin boundary condition.

Letting point x approach the boundary, we can obtain a conventional boundary integral equation referred to as CBIE:

$$c(x)p(x) + \int_S F(x,y)p(y)\,\mathrm{d}S(y) = \int_S G(x,y)q(y)\,\mathrm{d}S(y), \tag{5}$$

where x is the source point, y is the field point, the coefficient $c(x)$ is $1/2$ if S is smooth around the source point x, and $G(x,y)$ is the Green's function, $F(x,y)$ is the normal derivatives of $G(x,y)$. For 2D acoustic problems, the kernel functions are given as:

$$G(x,y) = \frac{i}{4}H_0^{(1)}(kr), \tag{6}$$

$$F(x,y) = \frac{\partial G(x,y)}{\partial n(y)} = -\frac{ik}{4}H_1^{(1)}(kr)\frac{\partial r}{\partial n(y)}, \tag{7}$$

where $r = |x-y|$, $H_n^{(1)}$ denotes the n-th order Hankel function of the first kind.

The CBIE formulation suffers from nonuniqueness for exterior problems. A remedy to this problem is to use CBIE in conjunction with its normal derivative equation.

Taking the derivative of the CBIE with respect to the outward normal at point x and letting x approach S if S is smooth around x, we obtain the following formulation usually referred to HBIE for acoustic wave problems:

$$\frac{1}{2}q(x) + \int_S \frac{\partial F(x,y)}{\partial n(x)}p(y)\,\mathrm{d}S(y) = \int_S \frac{\partial G(x,y)}{\partial n(x)}q(y)\,\mathrm{d}S(y). \tag{8}$$

For 2D acoustic problems, the two new kernel functions are given by:

$$\frac{\partial G(x,y)}{\partial n(x)} = -\frac{ik}{4}H_1^{(1)}(kr)\frac{\partial r}{\partial n(x)}, \tag{9}$$

$$\frac{\partial F(x,y)}{\partial n(x)} = \frac{ik}{4r}H_1^{(1)}(kr)n_j(x)n_j(y) + \frac{ik^2}{4}H_2^{(1)}(kr)\frac{\partial r}{\partial n(x)}\frac{\partial r}{\partial n(y)}. \tag{10}$$

The Burton-Miller formulation (Burton, Miller, 1971) using a linear combination of CBIE (5) and HBIE (8), as given below, should give a unique solution for all frequencies:

$$\text{CBIE} + \alpha\text{HBIE} = 0, \tag{11}$$

where α is the coupling constant, when $k \geq 1$, $\alpha = i/k$, but $\alpha = i$ for $k < 1$.

Assuming that the boundary S is discretised into boundary elements, the following system of linear algebraic equations can be obtained:

$$\mathbf{Hp} = \mathbf{Gq} + \mathbf{p}_\text{i}, \tag{12}$$

where $\mathbf{p}_\text{i}$ denotes the sound pressure from the incident wave.

For the HBIE formulation, the continuous elements (such as continuous linear element) may have difficulty of dealing with the normal vector of corner nodes, as shown in Fig. 1a. The normal vector of corner node i in actual smooth curvilinear boundary S is unique ($n(x)$ in Fig. 1a), but show discontinuity after discretisation.

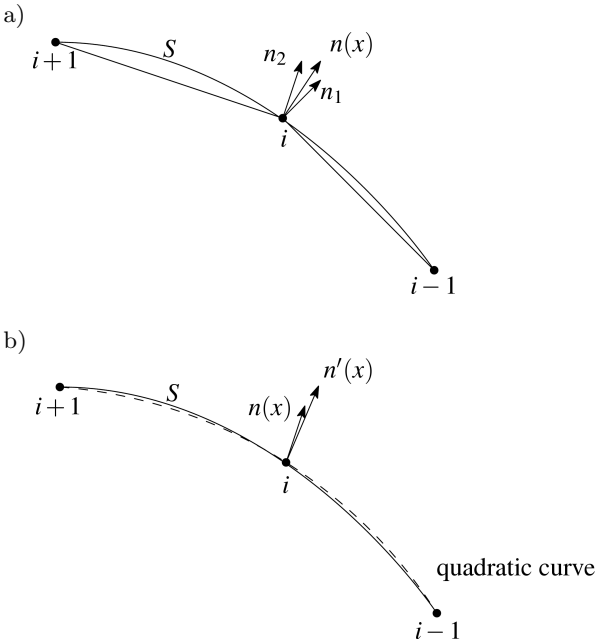

Fig. 1. Special treatment of the corner node of the continuous element.

The determination of accurate corner node normal vector according to the actual smooth curvilinear boundary S is always a high cost. Thus, special treatment of the corner nodes is required for continuous elements. As shown in Fig. 1b, we can obtain the normal vector of corner node i close to the accurate value by using a three noded $(i-1, i, i+1)$ quadratic curve instead of the actual boundary near the corner node.

Singular boundary integrals in Eqs. (5) and (8) can be evaluated explicitly and efficiently by using the Cauchy principal value and the Hadamard finite part integral method. The CBIE and HBIE formulations can be rewritten as:

$$\frac{1}{2}p(x) - \int_{S_x} G(x,y)q(y)\,\mathrm{d}S(y) = \int_{S\setminus S_x} G(x,y)q(y)\,\mathrm{d}S(y) - \int_{S\setminus S_x} F(x,y)p(y)\,\mathrm{d}S(y), \tag{13}$$

$$\frac{1}{2}q(x) + \int_{S_x} \frac{\partial F(x,y)}{\partial n(x)}p(y)\,\mathrm{d}S(y) = \int_{S\setminus S_x} \frac{\partial G(x,y)}{\partial n(x)}q(y)\,\mathrm{d}S(y) - \int_{S\setminus S_x} \frac{\partial F(x,y)}{\partial n(x)}p(y)\,\mathrm{d}S(y), \tag{14}$$

where S_x denotes the element containing the source point x, $S \setminus S_x$ denotes the boundary S except S_x. For different types of the element, we can obtain different expressions of singular parts in Eqs. (13) and (14), and the singular parts can be rewritten as:

$$\int_{S_x} G(x,y)q(y)\,\mathrm{d}S(y) = \int_{S_x} \left[G(\xi)J(\xi) - G_0(\xi)J_0(\xi)\right] q(\xi)\,\mathrm{d}\xi + \int_{S_x} G_0(\xi)J_0(\xi)q(\xi)\,\mathrm{d}\xi, \tag{15}$$

$$\int_{S_x} \frac{\partial F(x,y)}{\partial n(x)}p(y)\,\mathrm{d}S(y) = \int_{S_x} \left[F^1(\xi)J(\xi) - F_0^1(\xi)J_0(\xi)\right] p(\xi)\,\mathrm{d}\xi + \int_{S_x} F_0^1(\xi)J_0(\xi)p(\xi)\,\mathrm{d}\xi, \tag{16}$$

where ξ denotes the local coordinate in every element, J denotes the Jacobian, and

$$\begin{aligned} p(\xi) &= \sum_{i=1}^{n} \phi_i p_i, \\ q(\xi) &= \sum_{i=1}^{n} \phi_i q_i, \\ G_0(\xi) &= \lim_{x\to y} G(x,y) = -\frac{1}{2\pi}\ln(kr_0), \\ F_0^1(x,y) &= \lim_{x\to y}\left[\frac{ik}{4r}H_1^{(1)}(kr)n_j(x)n_j(y)\right] \\ &= \frac{1}{2kr_0^2} - \frac{k^2}{4\pi}\ln(kr_0), \\ J_0(\xi) &= \lim_{x\to y} J(\xi), \\ r^2 &= (\xi-b)^2 J, \\ r_0^2 &= (\xi-b)^2 J_0, \end{aligned} \tag{17}$$

where b denotes the local coordinate of the source point x. Eventually, the singular parts in Eqs. (15) and (16) can be rewritten as follows,

$$\begin{aligned} \int_{S_x} G_0(\xi)J_0(\xi)q(\xi)\,\mathrm{d}\xi &= \sum_{i=1}^{n} B_i q_i, \\ \int_{S_x} F_0^1(\xi)J_0(\xi)p(\xi)\,\mathrm{d}\xi &= \sum_{i=1}^{n} D_i p_i, \end{aligned} \tag{18}$$

where n denotes the number of interpolation nodes inside the boundary element.

By substituting Eq. (17) into Eq. (18), we can obtain the following formulation:

$$\begin{aligned} B_i &= -\frac{J_0}{2\pi}\ln(J_0 k)\int_{-1}^{1}\phi_i\,\mathrm{d}\xi \\ &\quad -\frac{J_0}{2\pi}\int_{-1}^{1}\phi_i\ln|\xi-b|\,\mathrm{d}\xi, \\ D_i &= -\frac{k^2 J_0}{4\pi}\ln(J_0 k)\int_{-1}^{1}\phi_i\,\mathrm{d}\xi \\ &\quad -\frac{k^2 J_0}{4\pi}\int_{-1}^{1}\phi_i\ln|\xi-b|\,\mathrm{d}\xi \\ &\quad +\frac{1}{2\pi J_0}\int_{-1}^{1}\frac{\phi_i}{(\xi-b)^2}\,\mathrm{d}\xi. \end{aligned} \tag{19}$$

Then, we can obtain the exact expressions of Eq. (19) by the Cauchy principal value and the Hadamard finite part integral method for different boundary element discretisation. For the constant element, $n=1$,

$$\begin{aligned} \phi_1 &= 1, \\ J_0(\xi) &= J(\xi) = \frac{L}{2}, \\ r(\xi) &= \frac{|\xi|L}{2}, \end{aligned} \tag{20}$$

where L is the length of each element. Thus,

$$\begin{aligned} B_1 &= -\frac{L}{2\pi}\left[\ln\left(\frac{kL}{2}\right)-1\right], \\ D_1 &= -\frac{k^2 L}{4\pi}\left[\ln\left(\frac{kL}{2}\right)+\frac{8}{k^2L^2}-1\right]. \end{aligned} \tag{21}$$

For the discontinuous linear element, $n=2$,

$$\begin{aligned} \phi_1 &= \frac{1}{2}\left(1-\frac{\xi}{a}\right), \\ \phi_2 &= \frac{1}{2}\left(1+\frac{\xi}{a}\right), \\ J_0(\xi) &= J(\xi) = \frac{L}{2}, \\ r(\xi) &= \frac{|\xi-b|L}{2}, \end{aligned} \tag{22}$$

where a $(0<a<1)$ decides the position of interpolation nodes, b denotes the local coordinate of the source point x. If $b=a$, then

$$\begin{aligned} B_1 &= -\frac{L}{2\pi}\ln\frac{kL}{2} - \frac{L}{8\pi a}\Pi_1, \\ B_2 &= -\frac{L}{2\pi}\ln\frac{kL}{2} - \frac{L}{8\pi a}\Pi_2, \\ D_1 &= \frac{\ln(1+a)-\ln(1-a)}{2a\pi L} \\ &\quad -\frac{k^2 L}{4\pi}\ln\frac{kL}{2} - \frac{k^2 L}{8\pi}\Pi_1, \\ D_2 &= \frac{\ln(1+a)-\ln(1-a)}{2a\pi L} - \frac{2}{\pi L(1-a^2)} \\ &\quad -\frac{k^2 L}{4\pi}\ln\frac{kL}{2} - \frac{k^2 L}{8\pi}\Pi_2, \end{aligned} \tag{23}$$

and

$$\begin{aligned} \Pi_1 &= \int_0^{1+a} x\ln x\,\mathrm{d}x - \int_0^{1-a} x\ln x\,\mathrm{d}x, \\ \Pi_2 &= \int_0^{1-a}\ln x\,\mathrm{d}x + \int_0^{1+a}\ln x\,\mathrm{d}x \\ &\quad -\frac{1}{2a}\left(\int_0^{1+a} x\ln x\,\mathrm{d}x - \int_0^{1-a} x\ln x\,\mathrm{d}x\right). \end{aligned} \tag{24}$$

And if $b=-a$, then B_1 and B_2, D_1 and D_2 will swap values, respectively.

For discontinuous quadratic element, $n=3$,

$$\begin{aligned}
\phi_1 &= \frac{\xi}{2a}\left(\frac{\xi}{a}-1\right),\\
\phi_2 &= 1-\frac{\xi^2}{a^2},\\
\phi_3 &= \frac{\xi}{2a}\left(\frac{\xi}{a}+1\right),\\
J^2(\xi) &= (A_1\xi+A_2)^2+(A_3\xi+A_4)^2,\\
J_0^2(\xi) &= (A_1 b+A_2)^2+(A_3 b+A_4)^2,\\
A_1 &= x_3^1-2x_2^1+x_1^1,\\
A_2 &= \frac{1}{2}(x_3^1-x_1^1),\\
A_3 &= x_3^2-2x_2^2+x_1^2,\\
A_4 &= \frac{1}{2}(x_3^2-x_1^2),\\
r^2 &= (\xi-b)^2J^2,\\
r_0^2 &= (\xi-b)^2J_0^2,
\end{aligned} \tag{25}$$

where $x_i^k(k=1,2)$ denotes the coordinates of the node $x_i(i=1,2,3)$ in each element.

There are three cases based on different values of b. When $b=0$, then

$$\begin{aligned}
B_1 &= -\frac{J_0}{2\pi}(\ln k+\ln J_0)\int_{-1}^{1}\phi_1\,\mathrm{d}\xi-\frac{J_0}{2\pi}\left(-\frac{1}{9a^2}\right),\\
B_2 &= -\frac{J_0}{2\pi}(\ln k+\ln J_0)\int_{-1}^{1}\phi_2\,\mathrm{d}\xi-\frac{J_0}{2\pi}\left(\frac{2}{9a^2}-2\right),\\
B_3 &= -\frac{J_0}{2\pi}(\ln k+\ln J_0)\int_{-1}^{1}\phi_3\,\mathrm{d}\xi-\frac{J_0}{2\pi}\left(-\frac{1}{9a^2}\right),\\
D_1 &= -\frac{k^2J_0}{4\pi}(\ln k+\ln J_0)\int_{-1}^{1}\phi_1\,\mathrm{d}\xi\\
&\quad+\frac{1}{2\pi J_0}\left(\frac{1}{a^2}\right)-\frac{k^2J_0}{4\pi}\left(-\frac{1}{9a^2}\right),\\
D_2 &= -\frac{k^2J_0}{4\pi}(\ln k+\ln J_0)\int_{-1}^{1}\phi_2\,\mathrm{d}\xi\\
&\quad+\frac{1}{2\pi J_0}\left(-\frac{2}{a^2}-2\right)-\frac{k^2J_0}{4\pi}\left(\frac{2}{9a^2}-2\right),\\
D_3 &= -\frac{k^2J_0}{4\pi}(\ln k+\ln J_0)\int_{-1}^{1}\phi_3\,\mathrm{d}\xi\\
&\quad+\frac{1}{2\pi J_0}\left(\frac{1}{a^2}\right)-\frac{k^2J_0}{4\pi}\left(-\frac{1}{9a^2}\right).
\end{aligned} \tag{26}$$

When $b=a$, then,

$$\begin{aligned}
B_1 &= -\frac{J_0}{2\pi}(\ln k+\ln J_0)\int_{-1}^{1}\phi_1\,\mathrm{d}\xi\\
&\quad-\frac{J_0}{2\pi}\left(\frac{1}{2a^2}(I_1+I_2)-\frac{1}{2a}I_3\right),\\
B_2 &= -\frac{J_0}{2\pi}(\ln k+\ln J_0)\int_{-1}^{1}\phi_2\,\mathrm{d}\xi\\
&\quad-\frac{J_0}{2\pi}\left(\frac{2}{a}I_3-\frac{1}{a^2}(I_1+I_2)\right),\\
B_3 &= -\frac{J_0}{2\pi}(\ln k+\ln J_0)\int_{-1}^{1}\phi_3\,\mathrm{d}\xi\\
&\quad-\frac{J_0}{2\pi}\left(\frac{1}{2a^2}(I_1+I_2)-\frac{3}{2a}I_3+(Y_1+Y_2)\right),\\
D_1 &= -\frac{k^2J_0}{4\pi}(\ln k+\ln J_0)\int_{-1}^{1}\phi_1\,\mathrm{d}\xi\\
&\quad+\frac{1}{2\pi J_0}\left(\frac{1}{a^2}+\frac{1}{2a}(\ln(1-a)-\ln(1+a))\right)\\
&\quad-\frac{k^2J_0}{4\pi}\left[\frac{1}{2a^2}(I_1+I_2)-\frac{1}{2a}I_3\right],\\
D_2 &= -\frac{k^2J_0}{4\pi}(\ln k+\ln J_0)\int_{-1}^{1}\phi_2\,\mathrm{d}\xi\\
&\quad+\frac{1}{2\pi J_0}\left(-\frac{2}{a^2}+\frac{2}{a}(\ln(1+a)-\ln(1-a))\right),\\
&\quad-\frac{k^2J_0}{4\pi}\left[\frac{2}{a}I_3-\frac{1}{a^2}(I_1+I_2)\right],\\
D_3 &= -\frac{k^2J_0}{4\pi}(\ln k+\ln J_0)\int_{-1}^{1}\phi_3\,\mathrm{d}\xi\\
&\quad+\frac{1}{2\pi J_0}\left(\frac{1}{a^2}+\frac{3}{2a}(\ln(1-a)-\ln(1+a))-\frac{2}{1-a^2}\right)\\
&\quad-\frac{k^2J_0}{4\pi}\left[\frac{1}{2a^2}(I_1+I_2)-\frac{3}{2a}I_3+(Y_1+Y_2)\right],
\end{aligned} \tag{27}$$

where

$$\begin{aligned}
I_1 &= \int_0^{1+a}x^2\ln x\,\mathrm{d}x, & I_2 &= \int_0^{1-a}x^2\ln x\,\mathrm{d}x,\\
X_1 &= \int_0^{1+a}x\ln x\,\mathrm{d}x, & X_2 &= \int_0^{1-a}x\ln x\,\mathrm{d}x,\\
I_3 &= X_1-X_2,\\
Y_1 &= \int_0^{1+a}\ln x\,\mathrm{d}x, & Y_2 &= \int_0^{1-a}\ln x\,\mathrm{d}x.
\end{aligned} \tag{28}$$

And if $b = -a$, then the value of B_1 and B_3, D_1 and D_3 of case $b = a$ will also change correspondingly.

2.2. FEM for structural domain

A harmonic load with the excitation frequency ω is assumed to be applied to the structure. The harmonic structural vibrations are described by

$$(\mathbf{K} + i\omega\mathbf{C} - \omega^2\mathbf{M})\mathbf{u}(\omega) = \mathbf{A}\mathbf{u} = \mathbf{f}, \tag{29}$$

where $i = \sqrt{-1}$, $\mathbf{K}$, $\mathbf{C}$, and $\mathbf{M}$ are respectively the stiffness matrix, damping matrix, and mass matrix for structure, structure matrix $\mathbf{A} = \mathbf{K} + i\omega\mathbf{C} - \omega^2\mathbf{M}$, $\mathbf{u}$ denotes the nodal displacement vector, and $\mathbf{f}$ is the nodal force vector. Considering the nodal forces $\mathbf{C}_{\mathrm{sf}}\mathbf{p}$ resulting from the acoustic pressure at the interaction surfaces, the excitation appears as:

$$\mathbf{f} = \mathbf{f_s} + \mathbf{C_{sf}}\mathbf{p}, \tag{30}$$

where the coupling matrix $\mathbf{C_{sf}}$ directs fluid nodal pressures to structural nodal forces, and it can be expressed as:

$$\mathbf{C}_{\mathrm{sf}} = \int_{S_{\mathrm{int}}} \mathbf{N}_{\mathrm{s}}^{\mathrm{T}}\mathbf{n}\mathbf{N}_{\mathrm{f}}\,\mathrm{d}S, \tag{31}$$

where S_{int} denotes the interaction surface, $\mathbf{N}_{\mathrm{s}}$ and $\mathbf{N}_{\mathrm{f}}$ are respectively the global shape functions of the structure and fluid domains, and $\mathbf{n}$ is the interaction surface normal vector.

By substituting Eq. (30) into Eq. (29), the nodal displacement vector can be written as:

$$\mathbf{u} = \mathbf{A}^{-1}\mathbf{f}_{\mathrm{s}} + \mathbf{A}^{-1}\mathbf{C}_{\mathrm{sf}}\mathbf{p}. \tag{32}$$

The governing equations Eqs. (29) and (12) are linked via the continuity condition $\mathbf{q} = -i\omega\rho\mathbf{v}$ across the interaction surface. Normal velocity $\mathbf{v}$ can be expressed as follows:

$$\mathbf{v} = i\omega\mathbf{S}^{-1}\mathbf{C}_{\mathrm{fs}}\mathbf{u}, \tag{33}$$

where

$$\mathbf{S} = \int_{S_{\mathrm{int}}} \mathbf{N}_{\mathrm{f}}^{\mathrm{T}}\mathbf{N}_{\mathrm{f}}\,\mathrm{d}S \qquad \text{and} \qquad \mathbf{C}_{\mathrm{fs}} = \mathbf{C}_{\mathrm{sf}}^{\mathrm{T}}.$$

By substituting Eq. (33) into Eq. (12), we can obtain the following formulation:

$$\mathbf{H}\mathbf{p} = \omega^2\rho\mathbf{G}\mathbf{S}^{-1}\mathbf{C}_{\mathrm{fs}}\mathbf{u} + \mathbf{p}_{\mathrm{i}}. \tag{34}$$

By combining Eq. (29) with Eq. (34), the governing equations for the coupled system can be given by

$$\begin{bmatrix} \mathbf{A} & -\mathbf{C}_{\mathrm{sf}} \\ -\omega^2\rho\mathbf{G}\mathbf{S}^{-1}\mathbf{C}_{\mathrm{fs}} & \mathbf{H} \end{bmatrix} \begin{Bmatrix} \mathbf{u} \\ \mathbf{p} \end{Bmatrix} = \begin{Bmatrix} \mathbf{f}_{\mathrm{s}} \\ \mathbf{p}_{\mathrm{i}} \end{Bmatrix}. \tag{35}$$

Directly solving Eq. (35) demands considerable computing time and storage requirement. The efficient method is substituting Eq. (29) into Eq. (34) to generate a reduced system equation, as follows:

$$\mathbf{H}\mathbf{p} - \mathbf{G}\mathbf{W}\mathbf{C}_{\mathrm{sf}}\mathbf{p} = \mathbf{G}\mathbf{W}\mathbf{f}_{\mathrm{s}} + \mathbf{p}_{\mathrm{i}}, \tag{36}$$

where $\mathbf{W} = \omega^2\rho\mathbf{S}^{-1}\mathbf{C}_{\mathrm{fs}}\mathbf{A}^{-1}$. The iterative solver GMRES and the FMM are applied to accelerating the calculation of the solution to the coupled boundary element system equation. Then we can obtain the nodal displacement vector by Eq. (32).

In this work, the wideband FMM approach is introduced to accelerate the calculation of the matrix-vector product in Eq. (36). Using conventional FMM (the low-frequency form) at a high frequency is inefficient because of a big truncation number, while employing diagonal FMM (the high-frequency form) at a low frequency exhibits a numerical instability problem. A remedy to the aforementioned problems is wideband FMBEM by combining conventional and diagonal forms. The details of the wideband FMM approach are presented in (Chen *et al.*, 2017).

3. Numerical examples

3.1. Element types

As compared with the constant element used in the previous acoustic BEM analysis, the continuous linear, quadratic, and discontinuous linear, quadratic elements for the 2D acoustic problem are developed in this study to achieve a higher accuracy.

For discontinuous elements, the interpolation nodes are located inside the element and the expressions of the shape functions depend on the position of the node inside the element. In Fig. 2, 'CBEmn' denotes the continuous boundary element with 'm' geometry nodes and 'n' interpolation nodes, and 'DBEmn' denotes the discontinuous boundary element with 'm' geometry nodes and 'n' interpolation nodes. For discontinuous boundary element, the value of a $(0 < a < 1)$ mentioned before decides about the position of the interpolation nodes. For the finite element, 'FE44' denotes

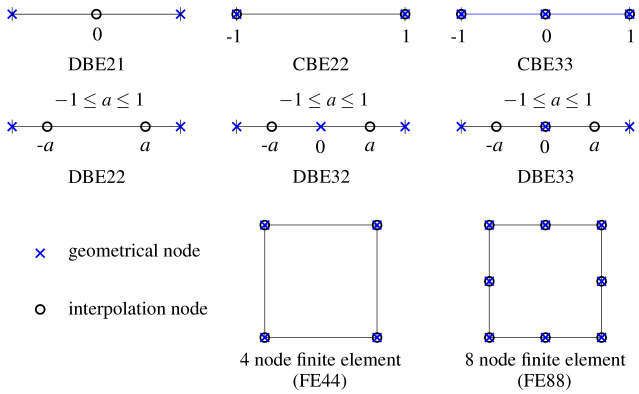

Fig. 2. Distribution of geometric nodes and interpolation nodes in the element.

the four-node isoparametric linear finite element, and 'FE88' denotes the eight-node isoparametric quadratic finite element.

3.2. Scattering from an infinite rigid cylindrical shell

In this example, we consider the acoustic scattering of a plane incident wave with a unit amplitude on a rigid cylindrical shell with radius $r_0 = 1.0$ m centered at point (0,0), as shown in Fig. 3.

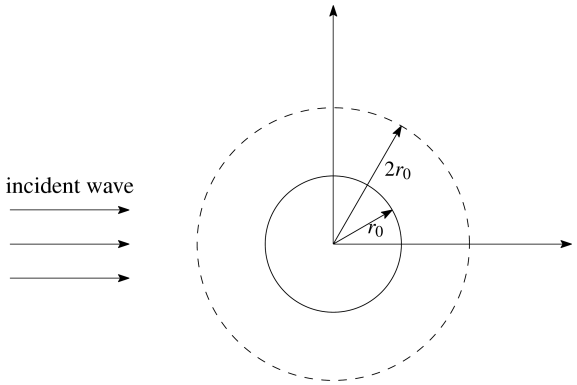

Fig. 3. Scattering from an innite cylindrical shell with radius r_0.

The analytical solution of the acoustic pressure at point (r, θ) is given as

$$p(r,\theta) = -\sum_{n=0}^{\infty} \varepsilon_n i^n \frac{J_n'(kr_0)}{H_n^{(1)'}(kr_0)} H_n^{(1)}(kr)\cos(n\theta), \quad (37)$$

where ε denotes the Neumann symbols, $\varepsilon_0 = 1$, $\varepsilon_n = 2$, $n > 0$; J_n denotes the n-th order Bessel function of the first kind; $()'$ denotes the differentiation with respect to kr_0.

360 sample internal points between $\theta = 0$ and $\theta = 2\pi$, evenly distributed on a circle of $r = 2.0$, are chosen. All the following relative errors are calculated based on the error function in (Marburg, Schneider, 2003).

In Fig. 4, "Rigid-analy" denotes the analytical solution of rigid analysis, "CBEM" denotes the numerical solution obtained by using the conventional BEM, and "FMBEM" denotes the numerical solution obtained by using the wideband fast multipole BEM. From this figure, it can be seen that the numerical solutions obtained by CBEM and FMBEM are in agreement with the analytical solution at the points on circle $r = 2r_0$ with $k = 1$.

The performance of different element types presented in the last subsection is evaluated by comparing the results using a similar number of geometric nodes. Figure 5 shows the performance of different element types with different mesh discretisation. It can be seen that the continuous element CBE22 performs most inefficiently, and the discontinuous element DBE33 performs most efficiently. And for the element with the

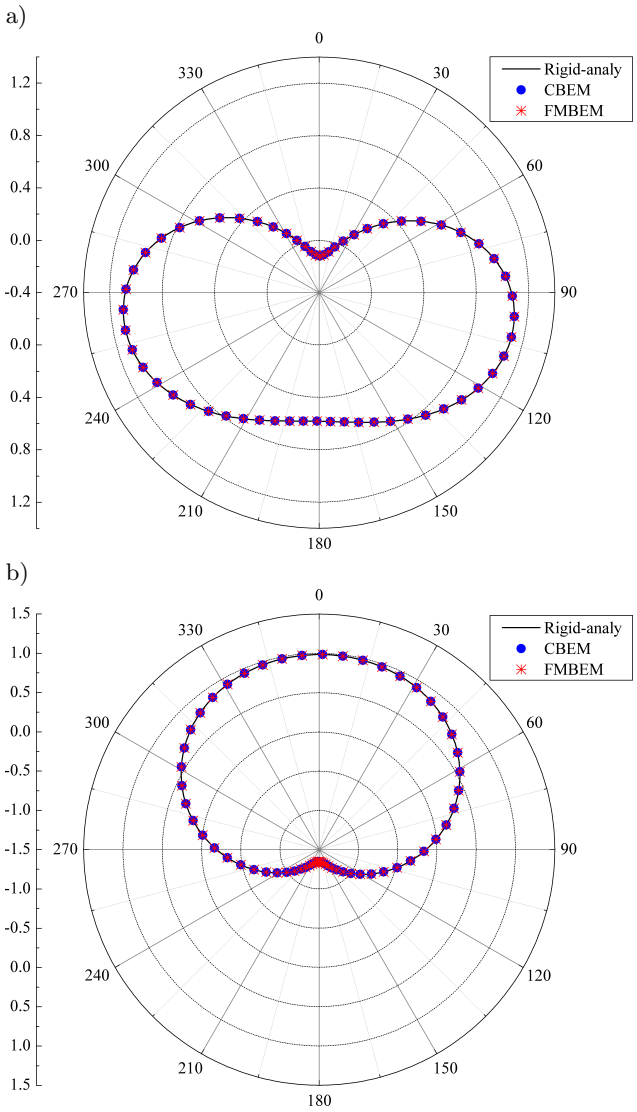

Fig. 4. Sound pressure at points on circle $r = 2.0$ with $k = 1$ of the rigid analysis: a) real part, b) imaginary part.

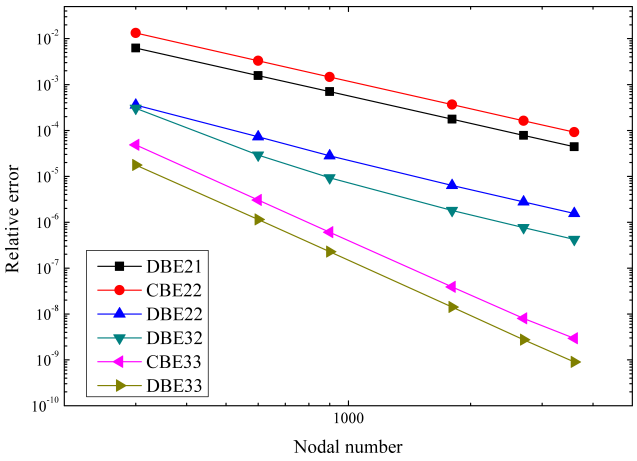

Fig. 5. Relative error in terms of nodal number for different types of elements at 5000 Hz.

same shape approximation as CBE33 and DBE33, the relative error varies similarly with the change of the

nodal number. In addition, the discontinuous elements perform better than the continuous elements, such as DBE22 and CBE22, DBE33 and CBE33.

Figure 6 shows the relative error in terms of the position of node for the linear element DBE22 at several frequencies. It can be seen that the optimal value for the nodal position has a small shift along with frequency, but the optimal value is always around 0.58, which is close to the zeros of the Legendre polynomial 0.5773.

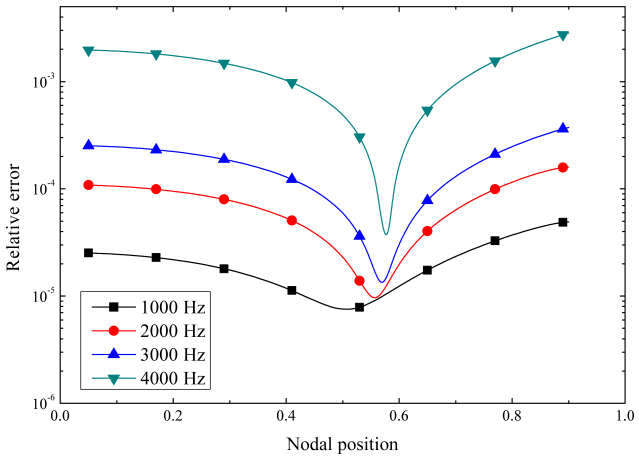

Fig. 6. Relative error in terms of the nodal position for DBE22 element.

Figure 7 shows the relative error in terms of the position of node for the quadratic element DBE33 at several frequencies. It can be seen that the optimal value for the nodal position has nearly no shift along with frequency and the optimal value is around 0.77, which is also close to the zeros of the Legendre polynomial 0.7746. In sum, it is the optimal value of the nodal position for DBE22 and DBE33 approach to the zeros of the Legendre polynomial. Besides, it can also be seen that a higher relative error happens for a higher frequency case.

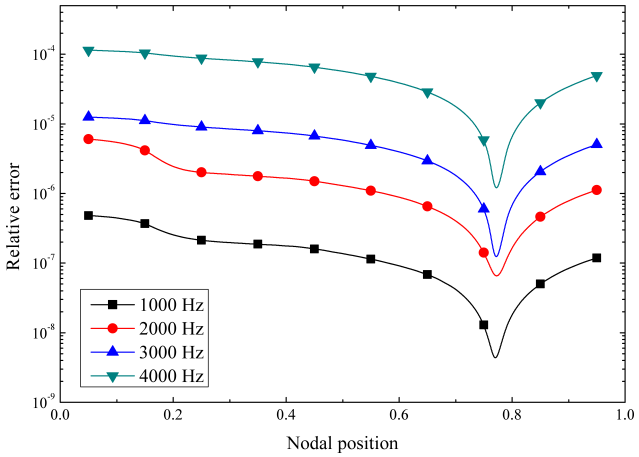

Fig. 7. Relative error in terms of the nodal position for DBE33 element.

As the problem size increases, it is necessary to develop preconditioning to the solution using an iterative solver (GMRES) for lower iteration numbers. In this work, the block diagonal preconditioner (Wu *et al.*, 2011) based on the FMM tree structure is applied. Figure 8 shows the iteration number for original and preconditioned cases in terms of frequency. It can be seen that the preconditioned iteration number is lower than the original case, and the preconditioning time in each iteration is negligible as compared with the time of the matrix-vector product. Through numerical tests, the iterative solution of the system of linear equation based on the GMRES method is determined to be the most time-consuming part of simulating models of practical problems by using the proposed algorithm. For complex practical problems, because the needed iteration time too high, the computational efficiency of the proposed algorithm will decrease fast. So, it is very important to improve the computational efficiency for practical problems by developing a suitable precondition method.

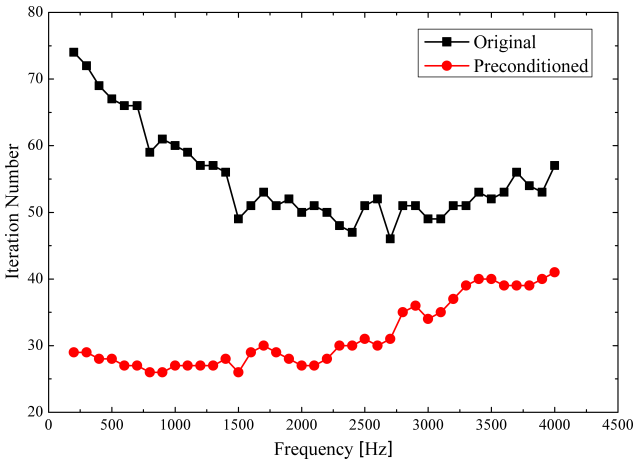

Fig. 8. Number of iteration relative to frequency.

Here, we consider the acoustic scattering of the same incident wave in Fig. 3 but with 4 rigid cylindrical shells of $r = 0.2$ m, as shown in Fig. 9.

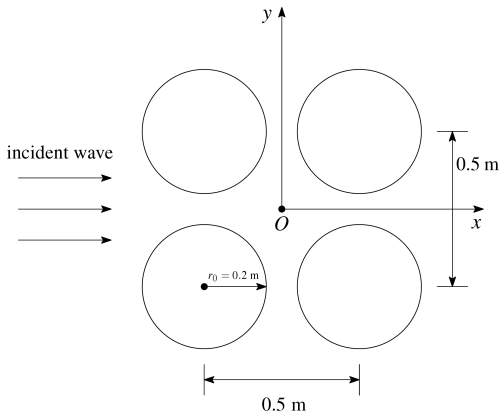

Fig. 9. Geometry of four infinite cylindrical shells with the frame and indicate wave.

360 sample internal points between $\theta = 0$ and $\theta = 360$, evenly distributed on a circle of $r = 2.0$, are chosen. Figure 10 shows the sound pressure at sample points with the wave number $k = 4.0$. From this figure, it can be seen that the numerical solutions obtained by FMBEM and CBEM are in good agreement.

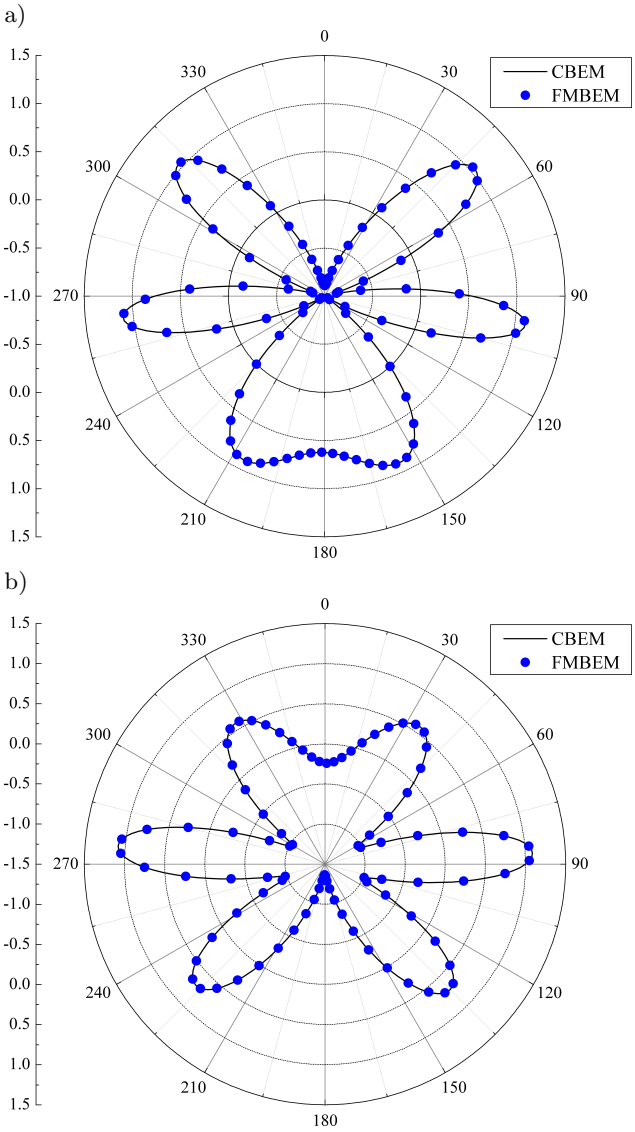

Fig. 10. Sound pressure at points on circle $r = 2$ with $k = 4$ of the rigid analysis: a) real part, b) imaginary part.

Figure 11 shows the sound pressure contour for scattering field for 4 cylindrical shells problems with the wave number $k = 4.0$.

Figure 12 shows the sound pressure contour for scattering of field for 400 rigid cylindrical shells problems with the wave number $k = 4.0$. FMBEM is applied to compute the acoustic scattering by multiple cylindrical shells with a plane incident wave with unit amplitude travelling along the positive x axis as shown in Fig. 12. The scattering model contains 400 random located cylinders in a square (1×1). Each cylinder is discretised with 1000 elements, and the number of all

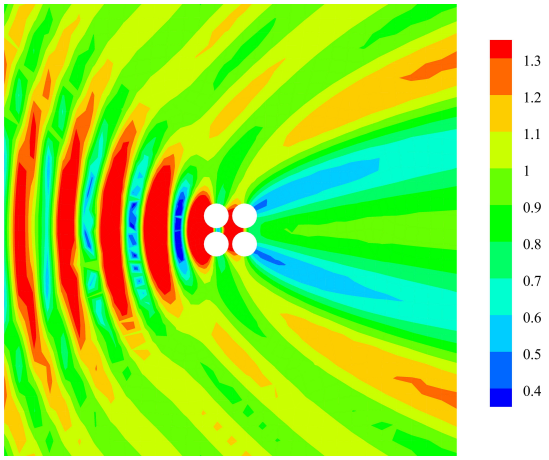

Fig. 11. Sound pressure contour plot for scattering of 4 rigid cylinders.

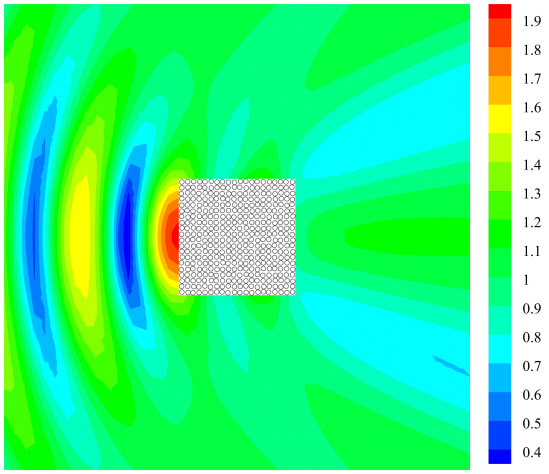

Fig. 12. Sound pressure contour plot for scattering of 400 rigid cylinders.

elements is 400 000. In addition, the near field outside the square is meshed with 3312 triangular elements.

3.3. Scattering from an infinite elastic cylindrical shell

To illustrate the method presented before, the acoustic scattering of a plane incident wave with a unit amplitude on an elastic cylindrical shell in water is modelled, as shown in Fig. 3. The material data and the geometrical data are listed in Table 1.

Table 1. Material and geometrical data for a elastic cylindrical shell.

Density (water)	ρ_f	1000	[kg/m^3]
Speed of sound (water)	c	1524	[m/s]
Density (steel)	ρ_s	7800	[kg/m^3]
Young's modulus (steel)	E	200	[GPa]
Poisson's ratio (steel)	ν	0.26	–
Radius of cylinder	r_0	1	[m]
Thickness of wall	t	0.05	[m]

An analytical series solution exists for this problem, and the sound pressure at point (r, θ) is given as

$$p(r,\theta) = -\sum_{n=0}^{\infty} \varepsilon_n i^n \frac{H_n^{(1)}(kr)}{H_n^{(1)'}(kr_0)} \cdot \left[J_n'(kr_0) - \frac{2\rho c}{(Z_n + z_n)\pi k r H_n^{(1)'}(kr_0)} \right] \cos(n\theta), \quad (38)$$

where the structure modal impedances Z_n and radiation impedances z_n are given by

$$Z_n = -\frac{i\rho_s c_p}{\Omega} \frac{h}{r} \frac{\left[\Omega^2 - (\Omega_n^{(1)})^2\right]\left[\Omega^2 - (\Omega_n^{(2)})^2\right]}{\Omega^2 - n^2}, \quad (39)$$

$$z_n = \frac{i\rho c H_n(kr_0)}{H_n'(kr_0)}, \quad (40)$$

where $c_p = [E/(1-\nu^2)\rho_s]^{1/2}$, $\Omega = \omega r_0/c_p$, and the eigen frequencies are

$$(\Omega_n^{(1)})^2 = \frac{1}{2}\Big[1 + n^2 + \beta^2 n^4 - \sqrt{(1+n^2+\beta^2 n^4)^2 - 4\beta^2 n^6}\Big], \quad (41)$$

$$(\Omega_n^{(2)})^2 = \frac{1}{2}\Big[1 + n^2 + \beta^2 n^4 + \sqrt{(1+n^2+\beta^2 n^4)^2 - 4\beta^2 n^6}\Big], \quad (42)$$

where $\beta^2 = h^2/(12r^2)$.

In Fig. 13, "Ela-analy" denotes the analytical solution of the elastic analysis, and "FEM/BEM" denotes the numerical solution obtained by using coupling FEM and BEM. From this figure, it can be seen that the numerical solution obtained by the coupling FEM/BEM is in good agreement with the analytical solution at the points on circle $r = 2r_0$ with $k = 1$. And by comparing with Fig. 4, the acoustic pressures of the elastic analysis at the points on circle $r = 2r_0$ differ from those of the rigid analysis.

Figure 14 shows a frequency comparison between the acoustic pressure values based on the rigid scattering and the elastic scattering, and the difference between the rigid and elastic solutions increases along with frequency. It means that the fluid has a big impact on the vibrating and scattering acoustic field of the underwater thin shell structure. From the two figures, it can also be seen that the numerical results obtained by the coupling FEM/BEM agree very well with the analytical solutions.

Figure 15 shows the relative error for FE44/DBE22 and FE88/DBE33 schemes at 500 Hz. From the figure it can be seen that FE88/DBE33 performs better than FE44/DBE22. It means that the higher shape function with the same linear shape approximation have nearly no improvement in accuracy, but using the quadratic

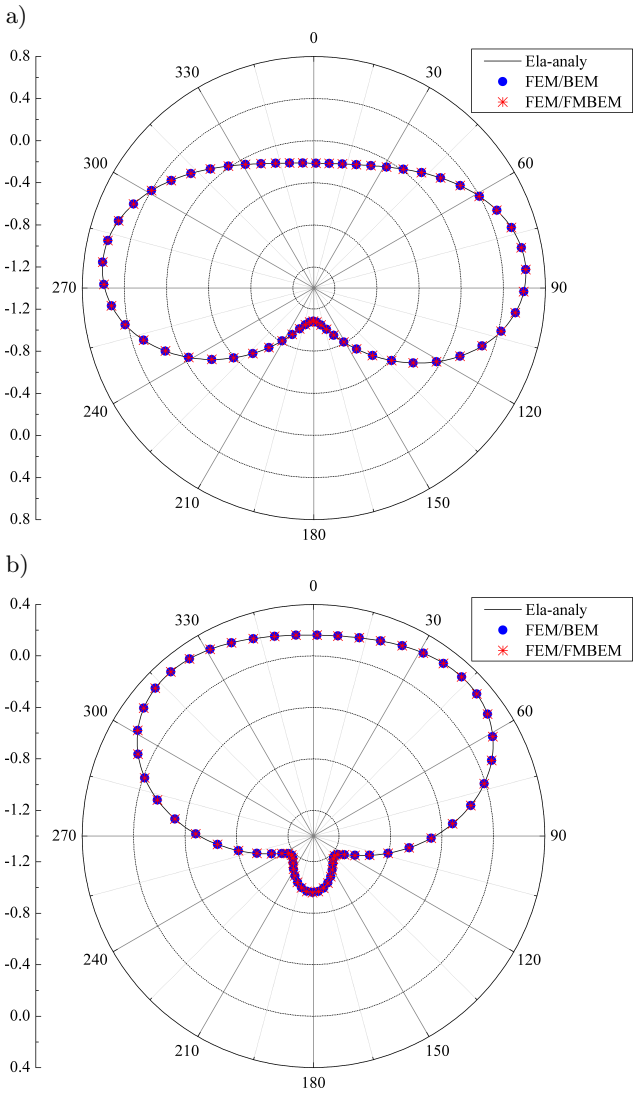

Fig. 13. Sound pressure at points on circle $r = 2r_0$ with $k = 1$ of the elastic analysis: a) real part, b) imaginary part.

shape approximation has an advantage over the linear one in accuracy. Thus, it is recommended to choose the quadratic shape function to obtain a higher accuracy.

Here, we also consider the elastic case of multiple domains, as shown in Fig. 9. Figure 16 shows the sound pressure at sample points with the wave number $k = 4.0$. From this figure it also can be seen that the numerical solutions obtained by FMBEM and CBEM are in good agreement with the elastic analysis, and the elastic solution differs from the rigid solution in Fig. 10. And Fig. 17 shows the sound pressure contour for scattering field of 4 cylindrical shells problem with the wave number $k = 4.0$, which is also quite different from Fig. 11 for the rigid analysis. When the fluid-structure interaction is taken into account, the scattering acoustic field consists of two parts. One is the pure scattering acoustic field from the rigid structure, another is the radiation acoustic field from the vibrating structure which is forced by the incident wave.

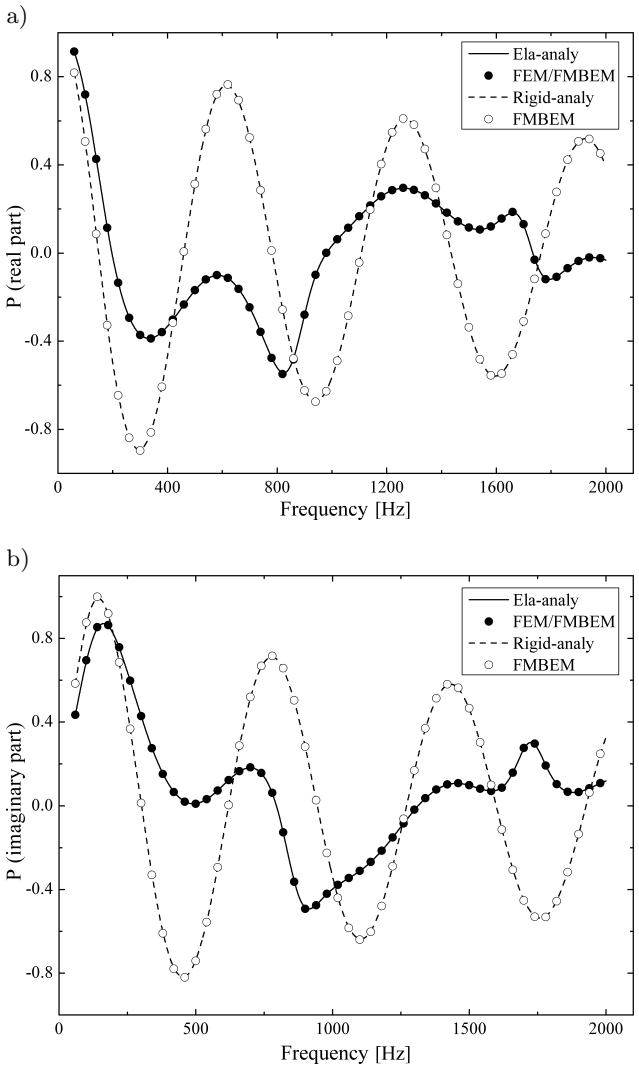

Fig. 14. Sound pressures at point $(2r_0, 0)$ with different frequencies.

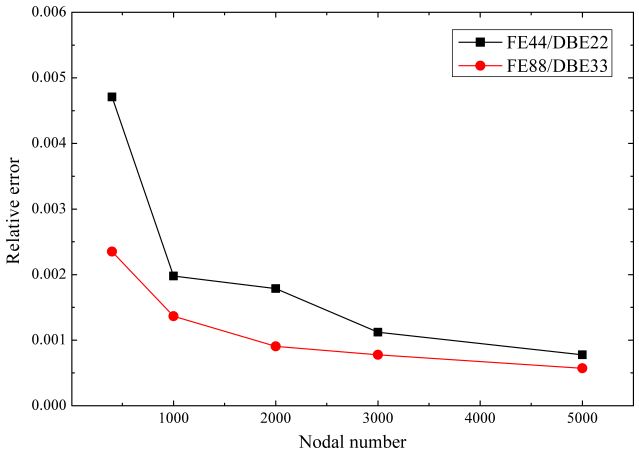

Fig. 15. Relative error in terms of the nodal number for different types of elements at 500 Hz.

When the structure is thin, the radiation acoustic field cannot be neglected. So, the scattering field in Fig. 17 is different from Fig. 11.

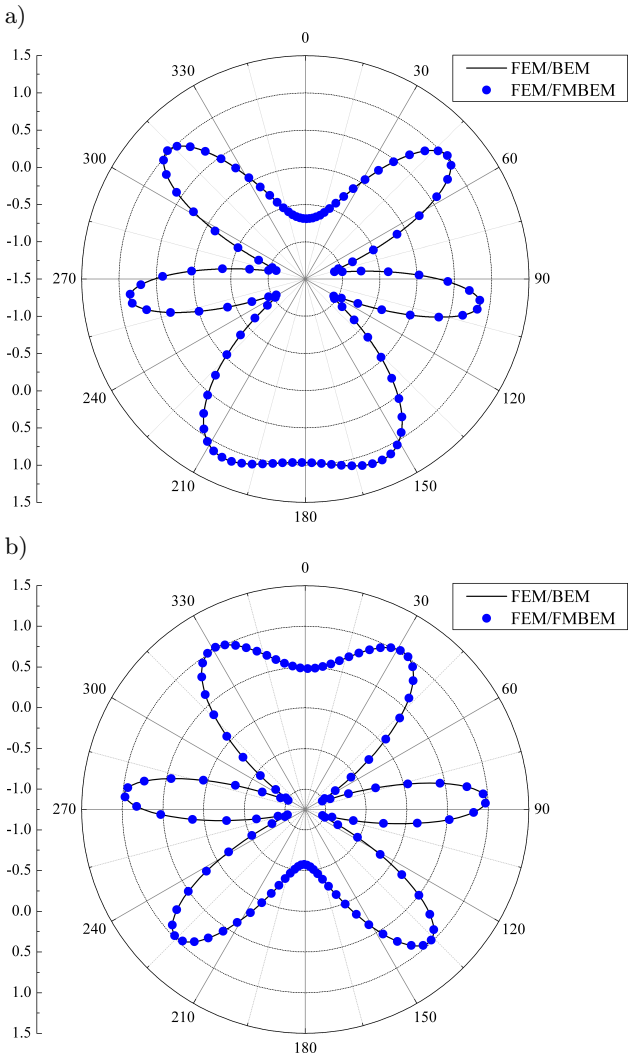

Fig. 16. Sound pressures at points on circle $r = 2$ with $k = 4$ of the elastic analysis.

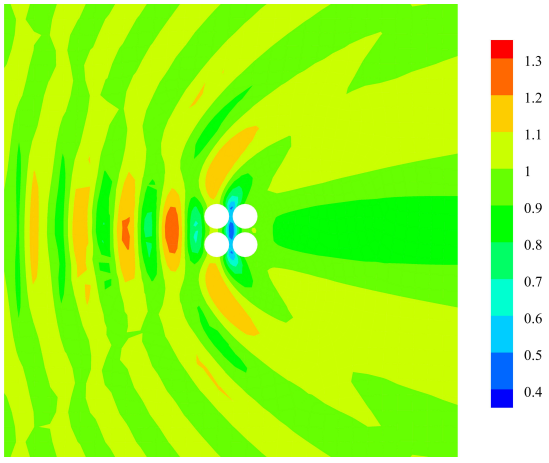

Fig. 17. Scattering from 4 infinite cylindrical shells with radius r_0.

4. Conclusion

A coupling algorithm based on FEM and FMBEM is presented for the simulation of fluid-structure inter-

action. In order to improve the accuracy, the singular integrals in boundary integral equations are evaluated by the Cauchy principal value and the Hadamard finite part integral method. Non-singular expressions of boundary integral equations for different boundary element types are also presented in this work. The FMM is used to accelerate the calculation of the matrix-vector products in the boundary element analysis. The proposed algorithm makes it possible to predict the effects of arbitrarily shaped vibrating structures on the sound field numerically. An example with the analytical solution is presented to demonstrate the correctness and validity of the proposed algorithm, and different coupled element schemes are compared. It can be seen that the discontinuous elements perform better than the continuous ones, and the optimal nodal value for discontinuous boundary elements is close to the zeros of the Legendre polynomial in the rigid analysis. On the other hand, the fluid has a big impact on the vibrating and scattering acoustic field of the underwater thin shell structure, and the coupled element with the quadratic shape approximation can improve the computational accuracy efficiently.

Future work includes applying the proposed algorithm to 3D practical engineering problems.

Acknowledgments

The financial support from the China Scholarship Council (CSC), National Natural Science Foundation of China (NSFC) under Grant no. 11172291, Research Fund for the Doctoral Program of Higher Education of China under Grand no. 20133402110036, and USTC under Grant no. WK2090000007 is acknowledged.

References

1. Burton A.J., Miller G.F. (1971), *The application of integral equation methods to the numerical solution of some exterior boundary-value problems*, Proceedings of the Royal Society of London A: Mathematical, Physical and Engineering Sciences, **323**, 1553, 201–210.
2. Chen L.L., Chen H.B. (2015), *Structural-acoustic design sensitivity analysis based on direct differentiation method with different element types*, CMES: Computer Modeling in Engineering & Sciences, **107**, 3, 249–276.
3. Chen L.L., Chen H.B., Zheng C.J. (2013a), *FEM/wideband FMBEM coupling for fluid-structure interaction problem and 2D acoustic design sensitivity analysis*, Comput. Model. Eng. Sci., **94**, 6, 459–483.
4. Chen Z.S., Hofstetter G., Mang H.A. (1998), *A Galerkin-type BE-FE formulation for elasto-acoustic coupling*, Computer Methods in Applied Mechanics and Engineering, **152**, 1–2, 147–155.
5. Chen L., Zheng C., Chen H. (2013b), *A wideband FMBEM for 2D acoustic design sensitivity analysis based on direct differentiation method*, Computational Mechanics, **52**, 3, 631–648.
6. Chen L., Zheng C., Chen H. (2014), *FEM/wideband FMBEM coupling for structural-acoustic design sensitivity analysis*, Computer Methods in Applied Mechanics and Engineering, **276**, 1–19.
7. Coifman R., Rokhlin V., Wandzura S. (1993), *The fast multipole method for the wave equation: a pedestrian prescription*, Antennas and Propagation Magazine, IEEE, **35**, 3, 7–12.
8. Everstine G.C., Henderson F.M. (1990), *Coupled finite element/boundary element approach for fluid-structure interaction*, The Journal of the Acoustical Society of America, **87**, 5, 1938–1947.
9. Fritze D., Marburg S., Hardtke H.-J. (2005), *FEM-BEM-coupling and structural-acoustic sensitivity analysis for shell geometries*, Computers & Structures, Advances in Analysis of Fluid Structure Interaction, **83**, 2–3, 143–154.
10. He Z.C., Liu G.R., Zhong Z.H., Zhang G.Y., Cheng A.G. (2011), *A coupled ES-FEM/BEM method for fluid-structure interaction problems*, Engineering Analysis with Boundary Elements, **35**, 1, 140–147.
11. Li S., Huang Q. (2011), *A new fast multipole boundary element method for two dimensional acoustic problems*, Computer Methods in Applied Mechanics and Engineering, **200**, 1333–1340.
12. Marburg S., Schneider S. (2003), *Influence of element types on numeric error for acoustic boundary elements*, Journal of Computational Acoustics, **11**, 03, 363–386.
13. Márquez A., Meddahi S., Selgas V. (2004), *A new BEM-FEM coupling strategy for two-dimensional fluid-solid interaction problems*, Journal of Computational Physics, **199**, 1, 205–220.
14. Peters H., Marburg S., Kessissoglou N. (2012), *Structural-acoustic coupling on non-conforming meshes with quadratic shape functions*, International Journal for Numerical Methods in Engineering, **91**, 1, 27–38.
15. Rajakumar C., Ali A. (1996), *Boundary elementfinite element coupled eigenanalysis of fluid-structure systems*, International Journal for Numerical Methods in Engineering, **39**, 10, 1625–1634.
16. Schneider S. (2008), *FE/FMBE coupling to model fluid-structure interaction*, International Journal for Numerical Methods in Engineering, **76**, 13, 2137–2156.
17. Tadeu A., António J. (2000), *Use of constant, linear and quadratic boundary elements in 3D wave diffraction analysis*, Engineering Analysis with Boundary Elements, **24**, 2, 131–144.
18. Yu C., Yu H., Chen Y. (2012), *Fast multipole boundary element method for 2-D Helmholtz equation problems and its error analysis*, Journal of Information & Computational Science, **9**, 18, 5571–5578.
19. Wu H., Jiang W., Liu Y.J. (2011), *Diagonal form fast multipole boundary element method for 2D acoustic problems based on Burton-Miller boundary integral equation formulation and its applications*, Applied Mathematics and Mechanics, **32**, 8, 981–996.
20. Zhang X., Zhang X. (2002), *Coupling FEM and discontinuous BEM for elastostatics and fluid-structure interaction*, Engineering Analysis with Boundary Elements, **26**, 8, 719–725.